Multiple Model Adaptive Estimation for Inertial Navigation During Mars Entry

Jeremy M. Marschke[*] John L. Crassidis[†]
University at Buffalo, State University of New York, Amherst, NY 14260-4400

Quang M. Lam[‡]
Orbital Sciences Corporation, Dulles, VA 20166

A multiple model adaptive estimation (MMAE) scheme is derived to determine both the position and the attitude of a vehicle during entry, descent and landing on Mars. MMAE uses several extended Kalman filters running in parallel, each representing a hypothesis of the actual system, to generate enhanced state and parameter estimates. The estimates of each parallel filter are combined based on the likelihood that each hypothesis is correct, which is determined from measurement residuals. The filter formulation is based on standard inertial navigation equations. The global attitude parameterization is given by a quaternion, while a generalized three-dimensional attitude representation is used to define the local attitude error. A multiplicative quaternion-error approach is used to guarantee that quaternion normalization is maintained in the filters. Three Kalman filters are used in the MMAE scheme: a 9 state filter, which includes attitude, position and velocity states, a 15 state filter, which adds gyro and accelerometer biases to the state state vector, and a 21 state filter, which adds gyro and accelerometer scale factors to the state vector. Simulation results are provided to show the effectiveness of the MMAE scheme.

I. Introduction

Future space missions currently envisioned by NASA Space Exploration Directorate that require landing on Moon (e.g., Orion), Mars, or asteroids are inherently challenging and demanding continuous mature technology insertion. Radio frequency communication delays rule out Earth-based remote control during entry, descent and landing (EDL). A high-accuracy 6-degree-of-freedom (DOF) navigation solution, a necessity for precise trajectory control during EDL, is difficult to obtain due to the absence of navigation aids such as GPS or radio beacons. Current EDL systems are based on the integration of acceleration and rotational velocity measurements from an inertial measurement unit (IMU). As with all forms of dead reckoning, navigation estimates obtained exclusively from an IMU are subject to relatively large error accumulations due to the integration of pure IMU data which contain various random noise sources (i.e., angular random walk, rate random walk, scale factor error, etc) and their associated biases. This error accumulation, when combined with uncertainties in surface-relative position and attitude at entry, has resulted in large landing error ellipses (e.g., for Mars Pathfinder, Mars Polar Lander, and the Mars Exploration Rovers) with axes of dimensions in the order of several hundred kilometers. Reducing the landing position uncertainty of future missions to several hundred meters accuracy or better (i.e., pin-point landing (PPL) capability or upcoming lunar landing accuracy) is of great importance and has been considered as the design goal (e.g., Autonomous Landing and Hazard Detection and Avoidance Program for Lunar Missions). This error growth becomes even bigger if a low-cost micro-electro-mechanical system (MEMS) IMU component is used.

One possible approach allowing future missions to meet precise navigation accuracy during EDL is to use onboard multiple external sensors (e.g., star tracker, altimeter, radar, ground cameras, etc.) as aiding

[*]Graduate Student, Department of Mechanical & Aerospace Engineering. Email: j253m@eng.buffalo.edu. Student Member AIAA.

[†]Professor, Department of Mechanical & Aerospace Engineering. Email: johnc@eng.buffalo.edu. Associate Fellow AIAA, Member AAS.

[‡]Chief Scientist, Orbital Sciences Corporation. Email: Lam.Quang@orbital.com. Senior Member AIAA, Member AAS.

sources to constantly correct/calibrate IMU noise source errors. The fusion of these multiple sensor updates using a typical single extended Kalman filter (EKF) design subject to their respective (different) update rates and sensor accuracy capacities (i.e., different measurement noise covariance) could potentially prevent the EKF from producing an adequate "navigation grade" to meet the PPL requirement. In addition, Mars atmospheric uncertainties may demand a more robust and adaptive navigation filter to be implemented onboard addressing and compensating for these variations/uncertainties.

Recent studies using an MMAE-based design scheme have demonstrated several key design features that are directly attractive and applicable to Mars missions, other space exploration missions, as well as uninhabited air vehicles.[1,2] These attractive MMAE based performance features include but are not limited to the following: (1) capable of compensating for both process noise and measurement noise uncertainties; (2) effectively and adaptively mixing/fusing information from multiple sources (i.e., IMU, star tracker, altimeter, etc.); (3) maximizing the "average quaternion" design enhancement principle, offering a 6DOF navigation solution averaging using the Adaptive Interacting Multiple Model (AIMM) mixing algorithm; and (4) the accommodation of a MEMS IMU system for future missions while being able to produce reliable and accurate navigation solutions.

A previous study of MMAE applied to Mars entry has been conducted by Zanetti and Bishop.[3] This study, however, is restricted to the multiple model estimation of the Martian atmospheric density in addition to position and attitude. IMU measurements are still assumed, but no corrections to these sensors are made. The scope of our paper study can be improved upon by adaptively estimating the process noise covariance, as well as sensor biases and scale factors.[2] Such additions increase the robustness and fidelity of the estimation scheme. This paper serves as a continuation effort to evaluate the MMAE navigation design concept, with the ultimate goal of eventually incorporating high fidelity truth data from a Mars mission.[1,2] These papers deal with only attitude estimation, while the present paper adds in position estimation as well. The work in Refs. 1 and 2 uses three basic filters: a 6 state filter, which includes attitude and gyro bias states, a 9 state filter, which adds gyro scale factors to the state state vector, and a 15 state filter, which adds gyro misalignments to the state vector. An MMAE algorithm is employed that uses a combination of all three filters. Conventional wisdom would assume that an actual system with all errors present would make the 15 state filter more accurate. However, the information dilution theorem[4] shows that adding extra estimation variables in a filter design can "stress" the Kalman filter, which may produce worse results than using a lower-order filter with errors present in the measurements or system. This is shown in Refs. 1 and 2 where the MMAE weights produced an overall estimate that is a function of all three filters, not just the 15 state filter, i.e. the 15 state filter did not have a weight of one.

II. Reference Frames

In this section the reference frames used to derive the inertial navigation system (INS) equations are summarized, as shown in Figure 1:

- Mars-Centered-Inertial (MCI) Frame: denoted by $\{\hat{\mathbf{i}}_1, \hat{\mathbf{i}}_2, \hat{\mathbf{i}}_3\}$. The $\hat{\mathbf{i}}_1$ axis points toward the Martian northern hemisphere vernal equinox direction, the $\hat{\mathbf{i}}_3$ axis points in the direction of the Martian North pole and the $\hat{\mathbf{i}}_2$ axis completes the right-handed system (note that the $\hat{\mathbf{i}}_1$ and $\hat{\mathbf{i}}_2$ axes are on the equator, which is the fundamental plane). The MCI frame is non-rotating with respect to the stars (except for precession of equinoxes) and Mars turns relative to this frame. Vectors described using MCI coordinates will have a superscript I (e.g., $\mathbf{r}^I$).

- Mars-Centered-Mars-Fixed (MCMF) Frame: denoted by $\{\hat{\mathbf{m}}_1, \hat{\mathbf{m}}_2, \hat{\mathbf{m}}_3\}$. This frame is similar to the MCI frame with $\hat{\mathbf{m}}_3 = \hat{\mathbf{i}}_3$; however, the $\hat{\mathbf{m}}_1$ axis points in the direction of the Martian prime meridian (defined as passing through the small crater Airy-0), and the $\hat{\mathbf{m}}_2$ axis completes the right-handed system. Unlike the MCI frame, the MCMF frame rotates with Mars. The rotation angle is denoted by Θ in Figure 1. Vectors described using MCMF coordinates will have a superscript M (e.g., $\mathbf{r}^M$).

- Body Frame: denoted by $\{\hat{\mathbf{b}}_1, \hat{\mathbf{b}}_2, \hat{\mathbf{b}}_3\}$. This frame is fixed onto the vehicle body and rotates with it. Conventions typically depend on the particular vehicle. Vectors described using body-frame coordinates will have a superscript B (e.g., $\mathbf{r}^B$).

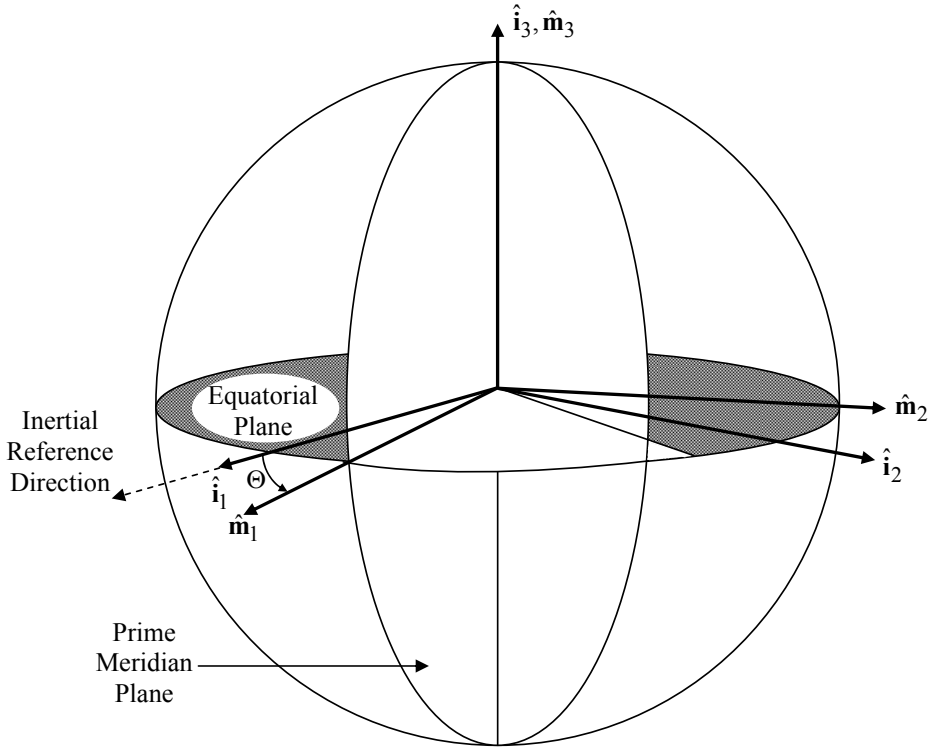

Figure 1. Definitions of Various Reference Frames

We now discuss the transformations between these reference frames. The transformation from the MCI frame to the MCMF frame follows

$$\begin{bmatrix} x \\ y \\ z \end{bmatrix}^M = \begin{bmatrix} \cos\Theta & \sin\Theta & 0 \\ -\sin\Theta & \cos\Theta & 0 \\ 0 & 0 & 1 \end{bmatrix} \begin{bmatrix} x \\ y \\ z \end{bmatrix}^I \tag{1}$$

where $\{x, y, z\}^I$ are the components of the MCI position vector, and $\{x, y, z\}^M$ are the components of the MCMF position vector. In order to determine the MCMF position vector we must first determine the angle Θ, which is related to time. A solar day is the length of time that elapses between the Sun reaching its highest point in the sky two consecutive times. However, the MCI coordinate system is fixed relative to the stars, not the Sun. A *sidereal day* is the length of time that passes between a given fixed star in the sky crossing a given projected meridian. A martian sidereal day is about 2 minutes shorter than a solar day. A conversion between martian siderial time and the rotation angle of the planet is straightforward to derive given an initial condition.

III. Attitude Kinematics

In this section the basic properties of attitude kinematics are summarized. The attitude matrix involves a total of nine parameters, but they are clearly not independent. Various parameterizations of the attitude matrix can be used: Euler angles, Euler axis and rotation angle, quaternions, Rodrigues parameters, etc.[5] One of the most useful attitude parameterization is given by the quaternion,[6] which is a four-dimensional vector, defined as $\mathbf{q} \equiv [\boldsymbol{\varrho}^T \ q_4]^T$, with $\boldsymbol{\varrho} \equiv [q_1 \ q_2 \ q_3]^T = \hat{\mathbf{e}} \sin(\vartheta/2)$ and $q_4 = \cos(\vartheta/2)$, where $\hat{\mathbf{e}}$ is the axis of rotation and ϑ is the angle of rotation. Since a four-dimensional vector is used to describe three dimensions, the quaternion components cannot be independent of each other. The quaternion satisfies a single constraint given by $\mathbf{q}^T\mathbf{q} = 1$, which is analogous to requiring that $\hat{\mathbf{e}}$ be a unit vector in the Euler axis/angle parameterization.[5] The attitude matrix that transform the inertial frame to the body frame is

related to the quaternion by

$$A_I^B(\mathbf{q}) = \Xi^T(\mathbf{q})\Psi(\mathbf{q}) \tag{2}$$

with

$$\Xi(\mathbf{q}) \equiv \begin{bmatrix} q_4 I_{3\times 3} + [\boldsymbol{\varrho}\times] \\ -\boldsymbol{\varrho}^T \end{bmatrix} \tag{3a}$$

$$\Psi(\mathbf{q}) \equiv \begin{bmatrix} q_4 I_{3\times 3} - [\boldsymbol{\varrho}\times] \\ -\boldsymbol{\varrho}^T \end{bmatrix} \tag{3b}$$

where $[\boldsymbol{\varrho}\times]$ is the cross product matrix, defined by

$$[\boldsymbol{\varrho}\times] \equiv \begin{bmatrix} 0 & -q_3 & q_2 \\ q_3 & 0 & q_1 \\ -q_2 & q_1 & 0 \end{bmatrix} \tag{4}$$

An advantage to using quaternions is that the attitude matrix is quadratic in the parameters and also does not involve transcendental functions. For small angles the vector part of the quaternion is approximately equal to half angles so that $\boldsymbol{\varrho} \approx \boldsymbol{\alpha}/2$ and $q_4 \approx 1$, where $\boldsymbol{\alpha}$ is a vector of the roll, pitch and yaw angles. The attitude matrix can then be approximated by

$$A_I^B \approx I_{3\times 3} - [\boldsymbol{\alpha}\times] \tag{5}$$

which is valid to within first-order in the angles.

The attitude kinematics equation is given by

$$\dot{A}_I^B = -[\boldsymbol{\omega}_{B/I}^B\times]A_I^B \tag{6}$$

where $\boldsymbol{\omega}_{B/I}^B$ is angular velocity of the B frame relative to the I frame expressed in B coordinates. Another form of Eq. (6) is given by

$$\dot{A}_B^I = A_B^I[\boldsymbol{\omega}_{B/I}^B\times] \tag{7}$$

which will be used in the derivation of the INS equations. The quaternion kinematics equation is given by

$$\dot{\mathbf{q}} = \frac{1}{2}\Xi(\mathbf{q})\boldsymbol{\omega}_{B/I}^B = \frac{1}{2}\Omega(\boldsymbol{\omega}_{B/I}^B)\mathbf{q} \tag{8}$$

where

$$\Omega(\boldsymbol{\omega}_{B/I}^B) \equiv \begin{bmatrix} -[\boldsymbol{\omega}_{B/I}^B\times] & \boldsymbol{\omega}_{B/I}^B \\ -(\boldsymbol{\omega}_{B/I}^B)^T & 0 \end{bmatrix} \tag{9}$$

The matrix $\Xi(\mathbf{q})$ obeys the following helpful relations:

$$\Xi^T(\mathbf{q})\Xi(\mathbf{q}) = (\mathbf{q}^T\mathbf{q})I_{3\times 3} \tag{10a}$$

$$\Xi(\mathbf{q})\Xi^T(\mathbf{q}) = (\mathbf{q}^T\mathbf{q})I_{4\times 4} - \mathbf{q}\,\mathbf{q}^T \tag{10b}$$

$$\Xi^T(\mathbf{q})\mathbf{q} = \mathbf{0}_{3\times 1} \tag{10c}$$

$$\Xi^T(\mathbf{q})\boldsymbol{\lambda} = -\Xi^T(\boldsymbol{\lambda})\mathbf{q} \quad \text{for any } \boldsymbol{\lambda}_{4\times 1} \tag{10d}$$

Also, another useful identity is given by

$$\Psi(\mathbf{q})\boldsymbol{\omega}_{B/I}^B = \Gamma(\boldsymbol{\omega}_{B/I}^B)\mathbf{q} \tag{11}$$

where

$$\Gamma(\boldsymbol{\omega}_{B/I}^B) \equiv \begin{bmatrix} [\boldsymbol{\omega}_{B/I}^B\times] & \boldsymbol{\omega}_{B/I}^B \\ -(\boldsymbol{\omega}_{B/I}^B)^T & 0 \end{bmatrix} \tag{12}$$

A major advantage of using quaternions is that the kinematics equation is linear in the quaternion and is also free of singularities. Another advantage of quaternions is that successive rotations can be accomplished using quaternion multiplication. Here we adopt the convention of Lefferts, Markley, and Shuster[7] who multiply the quaternions in the same order as the attitude matrix multiplication (in contrast to the usual convention established by Hamiliton[6]). Suppose we wish to perform a successive rotation. This can be written using

$$A(\mathbf{q}')A(\mathbf{q}) = A(\mathbf{q}' \otimes \mathbf{q}) \tag{13}$$

The composition of the quaternions is bilinear, with

$$\mathbf{q}' \otimes \mathbf{q} = \begin{bmatrix} \Psi(\mathbf{q}') & \mathbf{q}' \end{bmatrix} \mathbf{q} = \begin{bmatrix} \Xi(\mathbf{q}) & \mathbf{q} \end{bmatrix} \mathbf{q}' \tag{14}$$

Also, the inverse quaternion is defined by

$$\mathbf{q}^{-1} \equiv \begin{bmatrix} -\boldsymbol{\varrho} \\ q_4 \end{bmatrix} \tag{15}$$

Note that $\mathbf{q} \otimes \mathbf{q}^{-1} = [0 \;\; 0 \;\; 0 \;\; 1]^T$, which is the identity quaternion. A computationally efficient algorithm to extract the quaternion from the attitude matrix is given in Ref. 8. A more thorough review of the attitude representations shown in this section, as well as others, can be found in the excellent survey paper by Shuster[5] and in the book by Kuipers.[9]

IV. INS Basic Equations

In this section the basic INS equations to be used in a filter are derived. We choose to use the MCMF reference frame since latitude and longitude are not well defined for the general celestial body. We begin the derivation by first discussing the notion used to represent an attitude rotation from one frame to another, given by

$$\mathbf{r}^M = A_I^M \mathbf{r}^I \tag{16}$$

where A_I^M is the attitude matrix that rotates from the I frame to the M frame. The kinematics equation for the attitude matrix is given by

$$\dot{A}_M^I = A_M^I [\boldsymbol{\omega}_{M/I}^M \times] \tag{17}$$

where $\boldsymbol{\omega}_{M/I}^M$ is the angular velocity of the M frame relative to the I frame expressed in M coordinates. The angular velocity vector is simply given by $\boldsymbol{\omega}_{M/I}^M = [0 \;\; 0 \;\; \omega_m]^T$, where ω_m is Mars's rotation rate given as 7.08822×10^{-5} rad/sec.

The linear-motion dynamics are derived by applying Newton's law, expressed in inertial coordinates. This is given by

$$\ddot{\mathbf{r}}^I = \mathbf{a}^I + \mathbf{g}^I \tag{18}$$

where $\mathbf{r}^I$ is the position vector, $\mathbf{a}^I$ is the inertial acceleration, and $\mathbf{g}^I$ is the gravity vector. We wish to determine an equation for $\ddot{\mathbf{r}}^M$. This is accomplished by taking two time-derivatives of Eq. (16) and using Eq. (17), which leads to

$$\ddot{\mathbf{r}}^I = A_M^I [\boldsymbol{\omega}_{M/I}^M \times][\boldsymbol{\omega}_{M/I}^M \times]\mathbf{r}^M + A_M^I [\dot{\boldsymbol{\omega}}_{M/I}^M \times]\mathbf{r}^M + 2A_M^I [\boldsymbol{\omega}_{M/I}^M \times]\dot{\mathbf{r}}^M + A_M^I \ddot{\mathbf{r}}^M \tag{19}$$

Note that $\dot{\boldsymbol{\omega}}_{M/I}^M$ is zero, so this term can be ignored. Left multiplying Eq. (19) by A_I^M, defining $\mathbf{a}^M \equiv A_I^M \mathbf{a}^I$ and $\mathbf{g}^M \equiv A_I^M \mathbf{g}^I$, which are the acceleration and gravity given in MCMF coordinates, and solving for $\ddot{\mathbf{r}}^M$ gives

$$\ddot{\mathbf{r}}^M = -[\boldsymbol{\omega}_{M/I}^M \times][\boldsymbol{\omega}_{M/I}^M \times]\mathbf{r}^M - 2[\boldsymbol{\omega}_{M/I}^M \times]\dot{\mathbf{r}}^M + \mathbf{a}^M + \mathbf{g}^M \tag{20}$$

The gravity model is given by

$$\mathbf{g}^M = \frac{-\mu}{||\mathbf{r}^M||^3} \mathbf{r}^M \tag{21}$$

Note that that the only nonlinear appearing term in Eq. (20) is due to the gravity model.

Gyros and accelerometers measure the body frame relative to the inertial frame, expressed in body frame coordinates. Specifically, gyros measure $\boldsymbol{\omega}_{B/I}^B$ and accelerometers measure $\mathbf{a}^B$, where the superscript B

denotes the body frame. The attitude determined from the INS relates the MCMF frame to the body frame, with the kinematics given by

$$\dot{A}_M^B = -[\boldsymbol{\omega}_{B/M}^B \times] A_M^B \tag{22}$$

Note that this equation cannot be used directly with the gyro measurement. However, this problem can be overcome by using the following identity:

$$\boldsymbol{\omega}_{B/I}^B = \boldsymbol{\omega}_{B/M}^B + \boldsymbol{\omega}_{M/I}^B \tag{23}$$

Solving Eq. (23) for $\boldsymbol{\omega}_{B/M}^B$ and substituting $\boldsymbol{\omega}_{M/I}^B = A_M^B \boldsymbol{\omega}_{M/I}^M$ yields

$$\boldsymbol{\omega}_{B/M}^B = \boldsymbol{\omega}_{B/I}^B - A_M^B \boldsymbol{\omega}_{M/I}^M \tag{24}$$

Now Eq. (22) can be related to the gyro measurements. Instead of the attitude matrix, we wish to employ quaternions since they are more convenient. The attitude matrix is related to the quaternion by

$$A_M^B(\mathbf{q}) = \Xi^T(\mathbf{q}) \Psi(\mathbf{q}) \tag{25}$$

The quaternion kinematics equation are given by

$$\dot{\mathbf{q}} = \frac{1}{2} \Xi(\mathbf{q}) \boldsymbol{\omega}_{B/M}^B \tag{26}$$

which must be initialized with some *a prior* attitude.

The gyro measurement model is given by

$$\tilde{\boldsymbol{\omega}}_{B/I}^B = (I_{3\times 3} + \mathcal{K}_g) \boldsymbol{\omega}_{B/I}^B + \mathbf{b}_g + \boldsymbol{\eta}_{gv} \tag{27a}$$

$$\dot{\mathbf{b}}_g = \boldsymbol{\eta}_{gu} \tag{27b}$$

where $\mathbf{b}_g$ is the gyro "bias", $\mathcal{K}_g$ is a diagonal matrix of gyro scale factors, and $\boldsymbol{\eta}_{gv}$ and $\boldsymbol{\eta}_{gu}$ are zero-mean Gaussian white-noise processes with spectral densities given by $\sigma_{gv}^2 I_{3\times 3}$ and $\sigma_{gu}^2 I_{3\times 3}$, respectively. The accelerometer measurement model is given by

$$\tilde{\mathbf{a}}^B = (I_{3\times 3} + \mathcal{K}_g) \mathbf{a}^B + \mathbf{b}_a + \boldsymbol{\eta}_{av} \tag{28a}$$

$$\dot{\mathbf{b}}_a = \boldsymbol{\eta}_{au} \tag{28b}$$

where $\mathbf{b}_a$ is the accelerometer "bias", $\mathcal{K}_a$ is a diagonal matrix of accelerometer scale factors, and $\boldsymbol{\eta}_{av}$ and $\boldsymbol{\eta}_{au}$ are zero-mean Gaussian white-noise processes with spectral densities given by $\sigma_{av}^2 I_{3\times 3}$ and $\sigma_{au}^2 I_{3\times 3}$, respectively. We should note that most manufacturers give values for σ_{gv} and σ_{av}, but not σ_{gu} and σ_{au}. The scale factors are assumed to be small enough so that the approximation $(I + \mathcal{K})^{-1} \approx (I - \mathcal{K})$ is valid for both the gyros and acclerometers. Simulating gyro and accelerometer using computers is not easy since continuous measurements cannot be generated using digital computers. A discrete-time simulation is possible using the spectral densities.[10]

V. Extended Kalman Filter Equations

In this section the implementation equations for the EKF are shown. The truth equations are given by

$$\dot{\mathbf{q}} = \frac{1}{2} \Xi(\mathbf{q}) \boldsymbol{\omega}_{B/M}^B \tag{29a}$$

$$\boldsymbol{\omega}_{B/M}^B = (I_{3\times 3} - \mathcal{K}_g)(\tilde{\boldsymbol{\omega}}_{B/I}^B - \mathbf{b}_g - \boldsymbol{\eta}_{gv}) - A_M^B(\mathbf{q}) \boldsymbol{\omega}_{M/I}^M \tag{29b}$$

$$\ddot{\mathbf{r}}^M = -[\boldsymbol{\omega}_{M/I}^M \times][\boldsymbol{\omega}_{M/I}^M \times] \mathbf{r}^M - 2[\boldsymbol{\omega}_{M/I}^M \times] \dot{\mathbf{r}}^M + A_B^M(\mathbf{q}) \mathbf{a}^B + \mathbf{g}^M \tag{29c}$$

$$\mathbf{a}^B = (I_{3\times 3} - \mathcal{K}_a)(\tilde{\mathbf{a}}^B - \mathbf{b}_a - \boldsymbol{\eta}_{av}) \tag{29d}$$

$$\mathbf{g}^M = \frac{-\mu}{||\mathbf{r}^M||^3} \mathbf{r}^M \tag{29e}$$

$$\dot{\mathbf{b}}_g = \boldsymbol{\eta}_{gu} \tag{29f}$$

$$\dot{\mathbf{b}}_a = \boldsymbol{\eta}_{au} \tag{29g}$$

$$\dot{\mathbf{k}}_g = \mathbf{0} \tag{29h}$$

$$\dot{\mathbf{k}}_a = \mathbf{0} \tag{29i}$$

where $\mathbf{k}_g$ and $\mathbf{k}_a$ are the elements of the diagonal matrices $\mathcal{K}_g$ and $\mathcal{K}_a$, respectively.

The MMAE scheme uses several filters in parallel. Filter 1 estimates only attitude and position, filter 2 estimates sensor biases in addition to this, and filter 3 also estimates scale factors. The equations for these filters are given by

$$\dot{\hat{\mathbf{q}}} = \frac{1}{2}\Xi(\hat{\mathbf{q}})\hat{\boldsymbol{\omega}}^B_{B/M} \tag{30a}$$

$$\hat{\boldsymbol{\omega}}^B_{B/M} = (I_{3\times 3} - \hat{\mathcal{K}}_g)(\tilde{\boldsymbol{\omega}}^B_{B/I} - \hat{\mathbf{b}}_g) - A^B_M(\hat{\mathbf{q}})\boldsymbol{\omega}^M_{M/I} \tag{30b}$$

$$\ddot{\hat{\mathbf{r}}}^M = -[\boldsymbol{\omega}^M_{M/I}\times][\boldsymbol{\omega}^M_{M/I}\times]\hat{\mathbf{r}}^M - 2[\boldsymbol{\omega}^M_{M/I}\times]\dot{\hat{\mathbf{r}}}^M + A^M_B(\hat{\mathbf{q}})\hat{\mathbf{a}}^B + \hat{\mathbf{g}}^M \tag{30c}$$

$$\hat{\mathbf{a}}^B = (I_{3\times 3} - \hat{\mathcal{K}}_a)(\tilde{\mathbf{a}}^B - \hat{\mathbf{b}}_a) \tag{30d}$$

$$\hat{\mathbf{g}}^M = \frac{-\mu}{||\hat{\mathbf{r}}^M||^3}\hat{\mathbf{r}}^M \tag{30e}$$

$$\dot{\hat{\mathbf{b}}}_g = \mathbf{0} \tag{30f}$$

$$\dot{\hat{\mathbf{b}}}_a = \mathbf{0} \tag{30g}$$

$$\dot{\hat{\mathbf{k}}}_g = \mathbf{0} \tag{30h}$$

$$\dot{\hat{\mathbf{k}}}_a = \mathbf{0} \tag{30i}$$

Where filter 1 neglects Eqs. (30f), (30g), (30h) and (30i), filter 2 neglects Eqs. (30h) and (30i), and filter 3 uses all equations during the update stage. Note that the attitude matrix is coupled into the position now, which allows us to estimate the attitude from position measurements. The accuracy of these estimates, however, can be drastically improved by incorporating an attitude sensor in addition to the IMU.

We now derive the error equations, which are used in the EKF covariance propagation. The quaternion is linearized using a multiplicative approach.[7] First, an error quaternion is defined by

$$\boldsymbol{\delta}\mathbf{q} = \mathbf{q} \otimes \hat{\mathbf{q}}^{-1} \tag{31}$$

with $\boldsymbol{\delta}\mathbf{q} \equiv [\boldsymbol{\delta\varrho}^T \;\; \delta q_4]^T$, where the quaternion multiplication is defined by Eq. (14). The equivalent attitude error matrix is given by

$$A^B_M(\boldsymbol{\delta}\mathbf{q}) = A^B_M(\mathbf{q})\left[A^B_M(\hat{\mathbf{q}})\right]^T \tag{32}$$

If the error quaternion is "small" then to within first order we have $\boldsymbol{\delta\varrho} \approx \boldsymbol{\delta\alpha}/2$ and $\delta q_4 \approx 1$, where $\boldsymbol{\delta\alpha}$ is a small error-angle rotation vector. Also, the quaternion inverse is defined by Eq. (15). The linearized model error-kinematics follow[7]

$$\boldsymbol{\delta}\dot{\boldsymbol{\varrho}} = -[\hat{\boldsymbol{\omega}}^B_{B/M}\times]\boldsymbol{\delta\varrho} + \frac{1}{2}\boldsymbol{\delta\omega} \tag{33a}$$

$$\delta\dot{q}_4 = 0 \tag{33b}$$

where $\boldsymbol{\delta\omega} \equiv \boldsymbol{\omega}^B_{B/M} - \hat{\boldsymbol{\omega}}^B_{B/M}$. Note that the fourth error-quaternion component is constant. The first-order approximation, which assumes that the true quaternion is "close" to the estimated quaternion, gives $\delta q_4 \approx 1$. This allows us to reduce the order of the system in the EKF by one state. The linearization using Eq. (31) maintains quaternion normalization to within first-order if the estimated quaternion is "close" to the true quaternion, which is within the first-order approximation in the EKF.

Equation (33) uses the vector part of the quaternion. It is more convenient to use the attitude-error vector, $\boldsymbol{\delta\alpha} = 2\boldsymbol{\delta\varrho}$, which leads to

$$\boldsymbol{\delta}\dot{\boldsymbol{\alpha}} = -[\hat{\boldsymbol{\omega}}^B_{B/M}\times]\boldsymbol{\delta\alpha} + \boldsymbol{\delta\omega} \tag{34}$$

where $\boldsymbol{\delta\omega} \equiv \boldsymbol{\omega}^B_{B/M} - \hat{\boldsymbol{\omega}}^B_{B/M}$. Substituting Eqs. (29b) and (30b) into $\boldsymbol{\delta\omega}$ leads to

$$\begin{aligned}\boldsymbol{\delta\omega} = &-\Delta\mathbf{b}_g - \Delta\mathcal{K}_g\tilde{\boldsymbol{\omega}}^B_{B/I} + \mathcal{K}_g\mathbf{b}_g - \hat{\mathcal{K}}_g\hat{\mathbf{b}}_g \\ &- [A^B_M(\mathbf{q}) - A^B_M(\hat{\mathbf{q}})]\boldsymbol{\omega}^M_{M/I} - (I_{3\times 3} - \mathcal{K}_g)\boldsymbol{\eta}_{gv}\end{aligned} \tag{35}$$

where $\Delta\mathbf{b}_g \equiv \mathbf{b}_g - \hat{\mathbf{b}}_g$ and $\Delta\mathcal{K}_g \equiv \mathcal{K}_g - \hat{\mathcal{K}}_g$. We need to linearize $A^B_M(\mathbf{q}) - A^B_M(\hat{\mathbf{q}})$. Solving Eq. (32) for $A^B_M(\mathbf{q})$ and substituting the resulting expression into $A^B_M(\mathbf{q}) - A^B_M(\hat{\mathbf{q}})$ gives

$$A^B_M(\mathbf{q}) - A^B_M(\hat{\mathbf{q}}) = \left[A^B_M(\boldsymbol{\delta}\mathbf{q}) - I_{3\times 3}\right]A^B_M(\hat{\mathbf{q}}) \tag{36}$$

The error-attitude matrix is approximated by

$$A_M^B(\boldsymbol{\delta q}) \approx I_{3\times 3} - [\boldsymbol{\delta\alpha}\times] \tag{37}$$

Substituting Eq. (37) into Eq. (36) gives

$$A_M^B(\mathbf{q}) - A_M^B(\hat{\mathbf{q}}) = -[\boldsymbol{\delta\alpha}\times]A_M^B(\hat{\mathbf{q}}) \tag{38}$$

Substituting Eq. (38) into Eq. (35), and also substituting $\mathbf{b}_g = \hat{\mathbf{b}}_g + \Delta\mathbf{b}_g$ and $\mathcal{K}_g = \hat{\mathcal{K}}_g + \Delta\mathcal{K}_g$ into Eq. (35) gives

$$\begin{aligned}\boldsymbol{\delta\omega} = &-\Delta\mathbf{b}_g - \tilde{\Omega}_{B/I}^B\Delta\mathbf{k}_g + (\hat{\mathcal{K}}_g + \Delta\mathcal{K}_g)(\hat{\mathbf{b}}_g + \Delta\mathbf{b}_g) - \hat{\mathcal{K}}_g\hat{\mathbf{b}}_g \\ &+ [\boldsymbol{\delta\alpha}\times]A_M^B(\hat{\mathbf{q}})\boldsymbol{\omega}_{M/I}^M - (I_{3\times 3} - \hat{\mathcal{K}}_g - \Delta\mathcal{K}_g)\boldsymbol{\eta}_{gv}\end{aligned} \tag{39}$$

where $\tilde{\Omega}_{B/I}^B$ is a diagonal matrix of the elements of $\tilde{\boldsymbol{\omega}}$ and $\Delta\mathbf{k}_g$ is a vector of the diagonal elements of $\Delta\mathcal{K}_g$. Ignoring second-order terms in Eq. (39) yields

$$\boldsymbol{\delta\omega} = -(I_{3\times 3} - \hat{\mathcal{K}}_g)\Delta\mathbf{b}_g - (\tilde{\Omega}_{B/I}^B - \hat{B}_g)\Delta\mathbf{k}_g - [A_M^B(\hat{\mathbf{q}})\boldsymbol{\omega}_{M/I}^M\times]\boldsymbol{\delta\alpha} - (I_{3\times 3} - \hat{\mathcal{K}}_g)\boldsymbol{\eta}_{gv} \tag{40}$$

where $\hat{B}_g$ is a diagonal matrix of the elements of $\hat{\mathbf{b}}_g$. Substituting Eq. (40) into Eq. (34) yields

$$\begin{aligned}\boldsymbol{\delta\dot{\alpha}} = &-\left[\left(\hat{\boldsymbol{\omega}}_{B/M}^B + A_M^B(\hat{\mathbf{q}})\boldsymbol{\omega}_{M/I}^M\right)\times\right]\boldsymbol{\delta\alpha} - (I_{3\times 3} - \hat{\mathcal{K}}_g)\Delta\mathbf{b}_g \\ &- (\tilde{\Omega}_{B/I}^B - \hat{B}_g)\Delta\mathbf{k}_g - (I_{3\times 3} - \hat{\mathcal{K}}_g)\boldsymbol{\eta}_{gv}\end{aligned} \tag{41}$$

Equation (41) gives the governing equation for the attitude error.

To determine the error equation for position we first define the following error:

$$\Delta\mathbf{r}^M = \mathbf{r}^M - \hat{\mathbf{r}}^M \tag{42}$$

Taking two time derivatives of Eq. (42) and substituting Eqs. (29c) and (30c), also using Eqs. (29d) and (30d), into the resulting expression leads to

$$\begin{aligned}\Delta\ddot{\mathbf{r}}^M = &-[\boldsymbol{\omega}_{M/I}^M\times][\boldsymbol{\omega}_{M/I}^M\times]\Delta\mathbf{r}^M - 2[\boldsymbol{\omega}_{M/I}^M\times]\Delta\dot{\mathbf{r}}^M + \left[A_B^M(\mathbf{q}) - A_B^M(\hat{\mathbf{q}})\right]\tilde{\mathbf{a}}^B \\ &- [A_B^M(\mathbf{q})\mathcal{K}_a - A_B^M(\hat{\mathbf{q}})\hat{\mathcal{K}}_a]\tilde{\mathbf{a}}^B - A_B^M(\mathbf{q})\mathbf{b}_a + A_B^M(\hat{\mathbf{q}})\hat{\mathbf{b}}_a \\ &+ A_B^M(\mathbf{q})\mathcal{K}_a\mathbf{b}_a - A_B^M(\hat{\mathbf{q}})\hat{\mathcal{K}}_a\hat{\mathbf{b}}_a - A_B^M(\mathbf{q})(I_{3\times 3} - \mathcal{K}_a)\boldsymbol{\eta}_{av} + \Delta\mathbf{g}^M\end{aligned} \tag{43}$$

where $\Delta\mathbf{g}^M \equiv \mathbf{g}^M - \hat{\mathbf{g}}^M$. Taking the transpose of Eq. (38) gives

$$A_B^M(\mathbf{q}) - A_B^M(\hat{\mathbf{q}}) = A_B^M(\hat{\mathbf{q}})[\boldsymbol{\delta\alpha}\times] \tag{44}$$

Therefore, $\left[A_B^M(\mathbf{q}) - A_B^M(\hat{\mathbf{q}})\right]\tilde{\mathbf{a}}^B$ in Eq. (43) becomes

$$\left[A_B^M(\mathbf{q}) - A_B^M(\hat{\mathbf{q}})\right]\tilde{\mathbf{a}}^B = -A_B^M(\hat{\mathbf{q}})[\tilde{\mathbf{a}}^B\times]\boldsymbol{\delta\alpha} \tag{45}$$

Next, we work on the expression $-[A_B^M(\mathbf{q})\mathcal{K}_a - A_B^M(\hat{\mathbf{q}})\hat{\mathcal{K}}_a]\tilde{\mathbf{a}}^B$ in Eq. (43). Using Eq. (44) and $\mathcal{K}_g = \hat{\mathcal{K}}_g + \Delta\mathcal{K}_g$ in this expression, and ignoring second-order terms yields

$$-[A_B^M(\mathbf{q})\mathcal{K}_a - A_B^M(\hat{\mathbf{q}})\hat{\mathcal{K}}_a]\tilde{\mathbf{a}}^B = -A_B^M(\hat{\mathbf{q}})\tilde{\mathcal{A}}^B\Delta\mathbf{k}_a + A_B^M(\hat{\mathbf{q}})[\hat{\mathcal{K}}_a\tilde{\mathbf{a}}^B\times]\boldsymbol{\delta\alpha} \tag{46}$$

where $\tilde{\mathcal{A}}^B$ is a diagonal matrix of the elements of $\tilde{\mathbf{a}}^B$ and $\Delta\mathbf{k}_a$ is a vector of the diagonal elements of $\Delta\mathcal{K}_a$. In a similar fashion we can show that to within first-order

$$-A_B^M(\mathbf{q})\mathbf{b}_a + A_B^M(\hat{\mathbf{q}})\hat{\mathbf{b}}_a = -A_B^M(\hat{\mathbf{q}})\Delta\mathbf{b}_a + A_B^M(\hat{\mathbf{q}})[\hat{\mathbf{b}}_a\times]\boldsymbol{\delta\alpha} \tag{47a}$$

$$A_B^M(\mathbf{q})\mathcal{K}_a\mathbf{b}_a - A_B^M(\hat{\mathbf{q}})\hat{\mathcal{K}}_a\hat{\mathbf{b}}_a = A_B^M(\hat{\mathbf{q}})\hat{\mathcal{K}}_a\Delta\mathbf{b}_a + A_B^M(\hat{\mathbf{q}})\hat{B}_a\Delta\mathbf{k}_a + A_B^M(\hat{\mathbf{q}})[\hat{\mathcal{K}}_a\mathbf{b}_a\times]\boldsymbol{\delta\alpha} \tag{47b}$$

$$A_B^M(\mathbf{q})(I_{3\times 3} - \mathcal{K}_a)\boldsymbol{\eta}_{av} = A_B^M(\hat{\mathbf{q}})(I_{3\times 3} - \hat{\mathcal{K}}_a)\boldsymbol{\eta}_{av} \tag{47c}$$

where $\hat{B}_a$ is a diagonal matrix of the elements of $\hat{\mathbf{b}}_a$. The final expression we require is the perturbation in the gravity difference $\Delta\mathbf{g}^M$ in Eq. (43). This is easily accomplished using a first-order Taylor series expansion, which yields

$$\Delta\mathbf{g}^M = U(\hat{\mathbf{r}}^M)\,\Delta\mathbf{r}^M \tag{48}$$

where

$$U(\hat{\mathbf{r}}^M) \equiv -\mu\left(I_{3\times3}\left|\left|\hat{\mathbf{r}}^M\right|\right|^{-3} - 3(\hat{\mathbf{r}}^M)(\hat{\mathbf{r}}^M)^T\left|\left|\hat{\mathbf{r}}^M\right|\right|^{-5}\right) \tag{49}$$

which is the gravity gradient expression. Finally, substituting Eqs. (45), (46), (47) and (48) into Eq. (43) gives

$$\begin{aligned}\Delta\ddot{\mathbf{r}}^M = &\left\{U(\hat{\mathbf{r}}^M) - [\boldsymbol{\omega}^M_{M/I}\times][\boldsymbol{\omega}^M_{M/I}\times]\right\}\Delta\mathbf{r}^M - 2[\boldsymbol{\omega}^M_{M/I}\times]\Delta\dot{\mathbf{r}}^M \\ &- A^M_B(\hat{\mathbf{q}})[\hat{\mathbf{a}}^B\times]\boldsymbol{\delta\alpha} - A^M_B(\hat{\mathbf{q}})(I_{3\times3} - \hat{\mathcal{K}}_a)\Delta\mathbf{b}_a \\ &- A^M_B(\hat{\mathbf{q}})(\tilde{\mathcal{A}}^B - \hat{B}_a)\Delta\mathbf{k}_a - A^M_B(\hat{\mathbf{q}})(I_{3\times3} - \hat{\mathcal{K}}_a)\boldsymbol{\eta}_{av}\end{aligned} \tag{50}$$

where $\hat{\mathbf{a}}^B$ is given by Eq. (30d). Equation (50) gives the governing equation for the acceleration error.

The state $\mathbf{x}_n$ and state-error vector $\Delta\mathbf{x}_n$ used in filter n are defined as

$$\mathbf{x}_1 \equiv \begin{bmatrix}\mathbf{q}\\ \mathbf{r}^M\\ \dot{\mathbf{r}}^M\end{bmatrix}, \quad \Delta\mathbf{x}_1 \equiv \begin{bmatrix}\boldsymbol{\delta\alpha}\\ \Delta\mathbf{r}^M\\ \Delta\dot{\mathbf{r}}^M\end{bmatrix} \tag{51a}$$

$$\mathbf{x}_2 \equiv \begin{bmatrix}\mathbf{q}\\ \mathbf{r}^M\\ \dot{\mathbf{r}}^M\\ \mathbf{b}_g\\ \mathbf{b}_a\end{bmatrix}, \quad \Delta\mathbf{x}_2 \equiv \begin{bmatrix}\boldsymbol{\delta\alpha}\\ \Delta\mathbf{r}^M\\ \Delta\dot{\mathbf{r}}^M\\ \Delta\mathbf{b}_g\\ \Delta\mathbf{b}_a\end{bmatrix} \tag{51b}$$

$$\mathbf{x}_3 \equiv \begin{bmatrix}\mathbf{q}\\ \mathbf{r}^M\\ \dot{\mathbf{r}}^M\\ \mathbf{b}_g\\ \mathbf{b}_a\\ \mathbf{k}_g\\ \mathbf{k}_a\end{bmatrix}, \quad \Delta\mathbf{x}_3 \equiv \begin{bmatrix}\boldsymbol{\delta\alpha}\\ \Delta\mathbf{r}^M\\ \Delta\dot{\mathbf{r}}^M\\ \Delta\mathbf{b}_g\\ \Delta\mathbf{b}_a\\ \Delta\mathbf{k}_g\\ \Delta\mathbf{k}_a\end{bmatrix} \tag{51c}$$

while the process noise vector and covariance are given by

$$\mathbf{w} \equiv \begin{bmatrix}\boldsymbol{\eta}_{gv}\\ \boldsymbol{\eta}_{gu}\\ \boldsymbol{\eta}_{av}\\ \boldsymbol{\eta}_{au}\end{bmatrix} \tag{52}$$

$$Q = \begin{bmatrix}\sigma^2_{gv}I_{3\times3} & 0_{3\times3} & 0_{3\times3} & 0_{3\times3}\\ 0_{3\times3} & \sigma^2_{gu}I_{3\times3} & 0_{3\times3} & 0_{3\times3}\\ 0_{3\times3} & 0_{3\times3} & \sigma^2_{av}I_{3\times3} & 0_{3\times3}\\ 0_{3\times3} & 0_{3\times3} & 0_{3\times3} & \sigma^2_{au}I_{3\times3}\end{bmatrix} \tag{53}$$

Hence, using Eqs. (41) and (50) as well as the gyro and accelerometer bias equations, the error-dynamics used in the EKF propagation of the n^{th} filter are given by

$$\Delta\dot{\mathbf{x}}_n = F_n\Delta\mathbf{x}_n + G_n\mathbf{w} \tag{54}$$

where

$$F_1 \equiv \begin{bmatrix} F_{11} & 0_{3\times3} & 0_{3\times3} \\ 0_{3\times3} & 0_{3\times3} & I_{3\times3} \\ F_{31} & F_{32} & F_{33} \end{bmatrix} \tag{55a}$$

$$G_1 \equiv \begin{bmatrix} -(I_{3\times3} - \hat{\mathcal{K}}_g) & 0_{3\times3} & 0_{3\times3} & 0_{3\times3} \\ 0_{3\times3} & 0_{3\times3} & 0_{3\times3} & 0_{3\times3} \\ 0_{3\times3} & 0_{3\times3} & -A_B^M(\hat{\mathbf{q}})(I_{3\times3} - \hat{\mathcal{K}}_a) & 0_{3\times3} \end{bmatrix} \tag{55b}$$

$$H_{1,k} = \begin{bmatrix} 0_{3\times3} & I_{3\times3} & 0_{3\times3} \end{bmatrix} \tag{55c}$$

$$F_2 \equiv \begin{bmatrix} F_{11} & 0_{3\times3} & 0_{3\times3} & F_{14} & 0_{3\times3} \\ 0_{3\times3} & 0_{3\times3} & I_{3\times3} & 0_{3\times3} & 0_{3\times3} \\ F_{31} & F_{32} & F_{33} & 0_{3\times3} & F_{35} \\ 0_{3\times3} & 0_{3\times3} & 0_{3\times3} & 0_{3\times3} & 0_{3\times3} \\ 0_{3\times3} & 0_{3\times3} & 0_{3\times3} & 0_{3\times3} & 0_{3\times3} \end{bmatrix} \tag{56a}$$

$$G_2 \equiv \begin{bmatrix} -(I_{3\times3} - \hat{\mathcal{K}}_g) & 0_{3\times3} & 0_{3\times3} & 0_{3\times3} \\ 0_{3\times3} & 0_{3\times3} & 0_{3\times3} & 0_{3\times3} \\ 0_{3\times3} & 0_{3\times3} & -A_B^M(\hat{\mathbf{q}})(I_{3\times3} - \hat{\mathcal{K}}_a) & 0_{3\times3} \\ 0_{3\times3} & I_{3\times3} & 0_{3\times3} & 0_{3\times3} \\ 0_{3\times3} & 0_{3\times3} & 0_{3\times3} & I_{3\times3} \end{bmatrix} \tag{56b}$$

$$H_{2,k} = \begin{bmatrix} 0_{3\times3} & I_{3\times3} & 0_{3\times3} & 0_{3\times3} & 0_{3\times3} \end{bmatrix} \tag{56c}$$

$$F_3 \equiv \begin{bmatrix} F_{11} & 0_{3\times3} & 0_{3\times3} & F_{14} & 0_{3\times3} & F_{16} & 0_{3\times3} \\ 0_{3\times3} & 0_{3\times3} & I_{3\times3} & 0_{3\times3} & 0_{3\times3} & 0_{3\times3} & 0_{3\times3} \\ F_{31} & F_{32} & F_{33} & 0_{3\times3} & F_{35} & 0_{3\times3} & F_{37} \\ 0_{3\times3} & 0_{3\times3} & 0_{3\times3} & 0_{3\times3} & 0_{3\times3} & 0_{3\times3} & 0_{3\times3} \\ 0_{3\times3} & 0_{3\times3} & 0_{3\times3} & 0_{3\times3} & 0_{3\times3} & 0_{3\times3} & 0_{3\times3} \\ 0_{3\times3} & 0_{3\times3} & 0_{3\times3} & 0_{3\times3} & 0_{3\times3} & 0_{3\times3} & 0_{3\times3} \\ 0_{3\times3} & 0_{3\times3} & 0_{3\times3} & 0_{3\times3} & 0_{3\times3} & 0_{3\times3} & 0_{3\times3} \end{bmatrix} \tag{57a}$$

$$G_3 \equiv \begin{bmatrix} -(I_{3\times3} - \hat{\mathcal{K}}_g) & 0_{3\times3} & 0_{3\times3} & 0_{3\times3} \\ 0_{3\times3} & 0_{3\times3} & 0_{3\times3} & 0_{3\times3} \\ 0_{3\times3} & 0_{3\times3} & -A_B^M(\hat{\mathbf{q}})(I_{3\times3} - \hat{\mathcal{K}}_a) & 0_{3\times3} \\ 0_{3\times3} & I_{3\times3} & 0_{3\times3} & 0_{3\times3} \\ 0_{3\times3} & 0_{3\times3} & 0_{3\times3} & I_{3\times3} \\ 0_{3\times3} & 0_{3\times3} & 0_{3\times3} & 0_{3\times3} \\ 0_{3\times3} & 0_{3\times3} & 0_{3\times3} & 0_{3\times3} \end{bmatrix} \tag{57b}$$

$$H_{3,k} = \begin{bmatrix} 0_{3\times3} & I_{3\times3} & 0_{3\times3} & 0_{3\times3} & 0_{3\times3} & 0_{3\times3} & 0_{3\times3} \end{bmatrix} \tag{57c}$$

with

$$F_{11} = -\left[\left(\hat{\boldsymbol{\omega}}^B_{B/M} + A^B_M(\hat{\mathbf{q}})\boldsymbol{\omega}^M_{M/I}\right)\times\right] \tag{58a}$$

$$F_{14} = -(I_{3\times3} - \hat{\mathcal{K}}_g) \tag{58b}$$

$$F_{16} = -(\tilde{\Omega}^B_{B/I} - \hat{B}_g) \tag{58c}$$

$$F_{31} = -A^M_B(\hat{\mathbf{q}})[\hat{\mathbf{a}}^B\times] \tag{58d}$$

$$F_{32} = U(\hat{\mathbf{r}}^M) - [\boldsymbol{\omega}^M_{M/I}\times][\boldsymbol{\omega}^M_{M/I}\times] \tag{58e}$$

$$F_{33} = -2[\boldsymbol{\omega}^M_{M/I}\times] \tag{58f}$$

$$F_{35} = -A^M_B(\hat{\mathbf{q}})(I_{3\times3} - \hat{\mathcal{K}}_a) \tag{58g}$$

$$F_{37} = -A^M_B(\hat{\mathbf{q}})(\tilde{\mathcal{A}}^B - \hat{B}_a) \tag{58h}$$

By using Eq. (57c), an implicit assumption is made that position observations are directly measured. For EDL on Mars, position measurements using a combination of data available from the Deep Space Network (DSN) and Mars Reconnaissance Orbiter (MRO) give a 1σ accuracy of about 300 meters.[11]

The EKF for INS estimation is summarized in Table 1. The assumed measurements are modeled by

$$\tilde{\mathbf{r}}^M_k = \mathbf{r}^M_k + \mathbf{v}_k \tag{59}$$

where $\mathbf{v}_k$ is a zero-mean Gaussian noise process with covariance given by R_k. The filter is first initialized with a known state (the bias initial conditions for the gyro and accelerometer are usually assumed zero) and error-covariance matrix. The first three diagonal elements of the error-covariance matrix correspond to attitude errors. Then, the Kalman gain is computed using the measurement-error covariance R_k and sensitivity matrix. The state error-covariance follows the standard EKF update. The position, velocity and bias states also follow the standard EKF additive correction while the attitude error-state update is computed using a multiplicative update.[7] Also, the updated quaternion is re-normalized by brute force. Finally, the propagation equations follow the standard EKF model. The process noise covariance is given in Eq. (51), and the matrices F and G are given in Eq. (53). Also, from Eqs. (30f) and (30g) the propagated bias estimates for the gyros and accelerometers are given by their respective updated values.

In order to reduce the computational load a discrete-time propagation of the covariance matrix can be used, given by

$$P^-_{k+1} = \Phi_k P^+_k \Phi^T_k + \mathcal{Q}_k \tag{60}$$

where Φ_k is the discrete-time state transition matrix and $\mathcal{Q}_k$ is the covariance matrix. A numerical solution for these matrices is given by van Loan.[12] First, the following matrix is formed:

$$\mathcal{A} = \begin{bmatrix} -F & G\,Q\,G^T \\ 0 & F^T \end{bmatrix}\Delta t \tag{61}$$

where Δt is the constant sampling interval. Then, the matrix exponential of Eq. (61) is computed:

$$\mathcal{B} = e^{\mathcal{A}} \equiv \begin{bmatrix} \mathcal{B}_{11} & \mathcal{B}_{12} \\ 0 & \mathcal{B}_{22} \end{bmatrix} = \begin{bmatrix} \mathcal{B}_{11} & \Phi^{-1}_k\mathcal{Q}_k \\ 0 & \Phi^T_k \end{bmatrix} \tag{62}$$

The state transition matrix is then given by

$$\Phi_k = \mathcal{B}^T_{22} \tag{63}$$

Also, the discrete-time process noise covariance is given by

$$\mathcal{Q}_k = \Phi_k\,\mathcal{B}_{12} \tag{64}$$

Note that this approach is only valid for time-invariant system and covariance matrices. Still, the approach can work well for time-varying matrices as long as the sampling rate is "fast" enough. The first-order approximation of Eq. (64) is given by $\Delta t\,G\,Q\,G^T$, which also is a good approximation if the sampling rate is fast.

Table 1. Extended Kalman Filter for (Loose) INS Estimation

Initialize	$\hat{\mathbf{x}}_n(t_0) = \hat{\mathbf{x}}_{n,0}$ $P_n(t_0) = P_{n,0}$
Gain	$K_{n,k} = P^-_{n,k} H^T_{n,k} [H_{n,k} P^-_{n,k} H^T_{n,k} + R_k]^{-1}$
Update	$P^+_{n,k} = [I - K_{n,k} H_{n,k}] P^-_{n,k}$ $\Delta\hat{\mathbf{x}}^+_{n,k} = K_{n,k}[\tilde{\mathbf{r}}^M_{n,k} - \hat{\mathbf{r}}^{M-}_{n,k}]$ $\hat{\mathbf{q}}^+_{n,k} = \hat{\mathbf{q}}^-_{n,k} + \frac{1}{2}\Xi(\hat{\mathbf{q}}^-_{n,k})\boldsymbol{\delta\hat{\alpha}}^+_{n,k}$, re-normalize quaternion $\hat{\mathbf{r}}^{M+}_{n,k} = \hat{\mathbf{r}}^{M-}_{n,k} + \Delta\hat{\mathbf{r}}^{M+}_{n,k}$ $\dot{\hat{\mathbf{r}}}^{M+}_{n,k} = \dot{\hat{\mathbf{r}}}^{M-}_{n,k} + \Delta\dot{\hat{\mathbf{r}}}^{M+}_{n,k}$ $\hat{\mathbf{b}}^+_{g_{n,k}} = \hat{\mathbf{b}}^-_{g_{n,k}} + \Delta\hat{\mathbf{b}}^+_{g_{n,k}}$ (filters 2 & 3 only) $\hat{\mathbf{b}}^+_{a_{n,k}} = \hat{\mathbf{b}}^-_{a_{n,k}} + \Delta\hat{\mathbf{b}}^+_{a_{n,k}}$ (filters 2 & 3 only) $\hat{\mathbf{k}}^+_{g_{n,k}} = \hat{\mathbf{k}}^-_{g_{n,k}} + \Delta\hat{\mathbf{k}}^+_{g_{n,k}}$ (filter 3 only) $\hat{\mathbf{k}}^+_{a_{n,k}} = \hat{\mathbf{k}}^-_{a_{n,k}} + \Delta\hat{\mathbf{k}}^+_{a_{n,k}}$ (filter 3 only)
Propagation	$\hat{\boldsymbol{\omega}}^B_{B/M} = (I_{3\times3} - \hat{\mathcal{K}}_g)(\tilde{\boldsymbol{\omega}}^B_{B/I} - \hat{\mathbf{b}}_g) - A^B_M(\hat{\mathbf{q}})\boldsymbol{\omega}^M_{M/I}$ $\dot{\hat{\mathbf{q}}} = \frac{1}{2}\Xi(\hat{\mathbf{q}})\,\hat{\boldsymbol{\omega}}^B_{B/M}$ $\hat{\mathbf{a}}^B = (I_{3\times3} - \hat{\mathcal{K}}_a)(\tilde{\mathbf{a}}^B - \hat{\mathbf{b}}_a)$ $\hat{\mathbf{g}}^M = \frac{-\mu}{\|\hat{\mathbf{r}}^M\|^3}\hat{\mathbf{r}}^M$ $\ddot{\hat{\mathbf{r}}}^M = -[\boldsymbol{\omega}^M_{M/I}\times][\boldsymbol{\omega}^M_{M/I}\times]\hat{\mathbf{r}}^M - 2[\boldsymbol{\omega}^M_{M/I}\times]\dot{\hat{\mathbf{r}}}^M + A^M_B(\hat{\mathbf{q}})\hat{\mathbf{a}}^B + \hat{\mathbf{g}}^M$ $\dot{P} = F\,P + P\,F^T + G\,Q\,G^T$

VI. Multiple-Model Adaptive Estimation

In this section a review of MMAE is shown. More details can be found in Refs. 13 and 14. Multiple-model adaptive estimation is a recursive estimator that uses a bank of filters that depend on some unknown parameters. In our case these parameters are the process noise covariance, denoted by the vector $\mathbf{p}$, which is assumed to be constant (at least throughout the interval of adaptation). Note that we do not necessarily need to make the stationary assumption for the state and/or output processes though, i.e. time varying state and output matrices can be used. A set of distributed elements is generated from some known pdf of $\mathbf{p}$, denoted by $p(\mathbf{p})$, to give $\{\mathbf{p}^{(\ell)};\, \ell = 1, \ldots, M\}$. The goal of the estimation process is to determine the conditional pdf of the ℓ^{th} element $\mathbf{p}^{(\ell)}$ given the current-time measurement $\tilde{\mathbf{y}}_k$. Application of Bayes' rule yields

$$p(\mathbf{p}^{(\ell)}|\tilde{\mathbf{Y}}_k) = \frac{p(\tilde{\mathbf{Y}}_k|\mathbf{p}^{(\ell)})\,p(\mathbf{p}^{(\ell)})}{\sum_{j=1}^{M} p(\tilde{\mathbf{Y}}_k|\mathbf{p}^{(j)})\,p(\mathbf{p}^{(j)})} \tag{65}$$

where $\tilde{\mathbf{Y}}_k$ denotes the sequence $\{\tilde{\mathbf{y}}_0, \tilde{\mathbf{y}}_1, \ldots, \tilde{\mathbf{y}}_k\}$. The *a posteriori* probabilities can be computed through[15]

$$\begin{aligned} p\left(\mathbf{p}^{(\ell)}|\tilde{\mathbf{Y}}_k\right) &= \frac{p\left(\tilde{\mathbf{y}}_k,\, \mathbf{p}^{(\ell)}|\tilde{\mathbf{Y}}_{k-1}\right)}{p\left(\tilde{\mathbf{y}}_k|\tilde{\mathbf{Y}}_{k-1}\right)} \\ &= \frac{p\left(\tilde{\mathbf{y}}_k|\hat{\mathbf{x}}_k^{-(\ell)}\right) p\left(\mathbf{p}^{(\ell)}|\tilde{\mathbf{Y}}_{k-1}\right)}{\sum_{j=1}^{M}\left[p\left(\tilde{\mathbf{Y}}_k|\hat{\mathbf{x}}_k^{-(j)}\right) p\left(\mathbf{p}^{(j)}|\tilde{\mathbf{Y}}_{k-1}\right)\right]} \end{aligned} \tag{66}$$

since $p\left(\tilde{\mathbf{y}}_k, |\tilde{\mathbf{Y}}_{k-1}, \mathbf{p}^{(\ell)}\right)$ is given by $p\left(\tilde{\mathbf{y}}_k|\hat{\mathbf{x}}_k^{-(\ell)}\right)$ in the Kalman recursion. Note that the denominator of Eq. (66) is just a normalizing factor to ensure that $p\left(\mathbf{p}^{(\ell)}|\tilde{\mathbf{Y}}_k\right)$ is a pdf. The recursion formula can now be cast into a set of defined weights $\varpi_k^{(\ell)}$, so that

$$\begin{aligned} \varpi_k^{(\ell)} &= \varpi_{k-1}^{(\ell)} p\left(\tilde{\mathbf{y}}_k|\hat{\mathbf{x}}_k^{-(\ell)}\right) \\ \varpi_k^{(\ell)} &\leftarrow \frac{\varpi_k^{(\ell)}}{\sum_{j=1}^{M}\varpi_k^{(j)}} \end{aligned} \tag{67}$$

where $\varpi_k^{(\ell)} \equiv p\left(\mathbf{p}^{(\ell)}|\tilde{\mathbf{y}}_k\right)$. The weights at time t_0 are initialized to $\varpi_0^{(\ell)} = 1/M$ for $\ell = 1, 2, \ldots, M$. The convergence properties of MMAE are shown in Ref. 15, which assumes ergodicity in the proof. The ergodicity assumptions can be relaxed to asymptotic stationarity and other assumptions are even possible for non-stationary situations.[16]

The conditional mean estimate is the weighted sum of the parallel filter estimates:

$$\hat{\mathbf{x}}_k^{-} = \sum_{j=1}^{M}\varpi_k^{(j)}\hat{\mathbf{x}}_k^{-(j)} \tag{68}$$

Also, the error covariance of the state estimate can be computed using

$$P_k^{-} = \sum_{j=1}^{M}\varpi_k^{(j)}\left[\left(\hat{\mathbf{x}}_k^{-(j)} - \hat{\mathbf{x}}_k^{-}\right)\left(\hat{\mathbf{x}}_k^{-(j)} - \hat{\mathbf{x}}_k^{-}\right)^T + P_k^{-(\ell)}\right] \tag{69}$$

The specific estimate for $\mathbf{p}$ at time t_k, denoted by $\hat{\mathbf{p}}_k$, and error covariance, denoted by $\mathcal{P}_k$, are given by

$$\hat{\mathbf{p}}_k = \sum_{j=1}^{M}\varpi_k^{(j)}\mathbf{p}^{(j)} \tag{70a}$$

$$\mathcal{P}_k = \sum_{j=1}^{M}\varpi_k^{(j)}\left(\mathbf{p}^{(j)} - \hat{\mathbf{p}}_k\right)\left(\mathbf{p}^{(j)} - \hat{\mathbf{p}}_k\right)^T \tag{70b}$$

Equation (70b) can be used to define 3σ bounds on the estimate $\hat{\mathbf{p}}_k$. For this paper no parameters are estimated since the MMAE scheme using a combination of three filters. Parameters, such as gyro noise variances, can also be estimated estimated in the MMAE if desired.

The likelihood function associated with the output residual is given by

$$p\left(\tilde{\mathbf{y}}_k|\hat{\mathbf{x}}_k^{-(\ell)}\right) = \frac{1}{\left\{\det[2\pi\left(H_k P_k^{-} H_k^T + R_k\right)]\right\}^{1/2}} \times \exp\left[-\frac{1}{2}\mathbf{e}_k^{(\ell)T}(H_k P_k^{-} H_k^T + R_k)^{-1}\mathbf{e}_k^{(\ell)}\right] \tag{71}$$

where $\mathbf{e}_k^{(\ell)} \equiv \tilde{\mathbf{y}}_k - \hat{\mathbf{y}}_k^{-(\ell)}$. For linear systems, such as the one in this paper, the estimate output is given by $\hat{\mathbf{y}}_k^{-(\ell)} = H_k\,\hat{\mathbf{x}}_k^{-(\ell)}$.

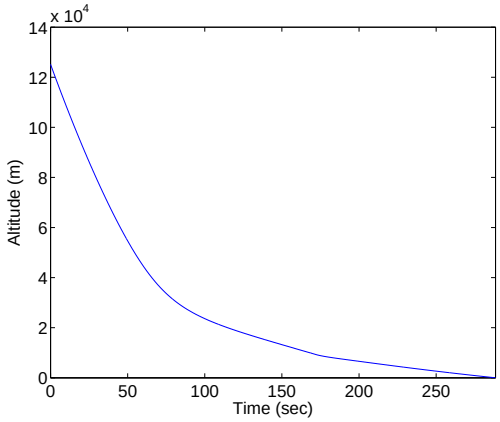

Figure 2. Simulation Altitude Profile

VII. Simulation Parameters

In order to verify the MMAE scheme, a navigation simulation during the EDL phase of a Mars mission is examined. The EDL simulation begins with the 900 kg spacecraft entering the Martian atmosphere ballistically at 125 km, with a speed of 7 km/s and a -14.0 deg flight path angle. The spacecraft experiences pure atmospheric deceleration, utilizing a (60 kg included) heat shield with $C_D = 1.7$, until it reaches 8 km. At this altitude, the heat shield is jettisoned and a parachute with $C_D = 0.41$ is deployed (no swinging simulated). The spacecraft lands on parachute at 0 km altitude.

Table 2. Simulation Parameters

Sampling Interval	$\Delta t = 0.100025$ sec
Gyro	$\sigma_{gv} = 0.001$ deg/hr$^{1/2}$ $\sigma_{gu} = 500 \times 10^{-6}$ rad/sec$^{3/2}$
Accelerometer	$\sigma_{av} = 0.4\mu g/\sqrt{\text{Hz}}$ $\sigma_{au} = 0$ m/sec$^{5/2}$
Initial Biases	$\mathbf{b}_g(t_0) = 500\,[1\ \ 1\ \ 1]^T \times 10^{-3}$ rad/s $\mathbf{b}_a(t_0) = 500\,[1\ \ 1\ \ 1]^T \times 10^{-3}$ g
Scale Factors	$\mathcal{K}_g = 500 I_{3\times 3}$ ppm $\mathcal{K}_a = 500 I_{3\times 3}$ ppm
Vehicle Origin	$\mathbf{r}^M(t_0) = [3522196\ \ 0\ \ 0]^T$ m
Initial Velocity	$\mathbf{v}^M(t_0) = [-1693.45\ \ -6792.07\ \ 0]^T$ m/s
Initial Attitude	$\mathbf{q}(t_0) = [.435\ \ .557\ \ .557\ \ .435]^T$

The vehicle motion is described in MCMF coordinates. Position measurements are obtained using a standard deviation of 300 meters for the white-noise errors. Throughout the simulation, attitude motion is 'shuttlecock', with the spacecraft central axis always oriented in the anti-drag direction. Mars is modeled as

a spherical body. The Martian atmosphere is modeled by:

$$\rho = \rho_0 e^{-h/h_0} \tag{72}$$

with $\rho_0 = 0.02$ kg/m^3 and $h_0 = 11$ km. All measurements are sampled every Δt seconds, and the total time of the simulation is 4 minutes and 48.47 seconds. The gyro noise parameters are given by σ_{gv} and σ_{gu}. The accelerometer parameters are given by σ_{av} and σ_{au}. Initial biases for the gyros and accelerometers are given by $\mathbf{b}_g(t_0)$ and $\mathbf{b}_a(t_0)$, respectively, for each axis. Also, $\mathcal{K}_g$ and $\mathcal{K}_a$ represent the gyro and accelerometer scale factors. The specific values of the simulation parameters are given in Table 2.

VIII. Simulation Results

In this section simulation results are shown that estimate for a moving vehicle's attitude, position and velocity as well as the gyro and accelerometer biases. Plots of the MMAE weights are shown in Figure 3. Note that all three filters are weighted nearly equally. This indicates that the 9 and 15 state filters do play an active role in the adaptive process to determine the overall best estimate. Figure 4 shows MMAE responses to initial condition (IC) conditions uncertainties, which gives different weights than the results shown in Figure 3. Plots of the MMAE results are shown in Figure 5. The attitude errors are shown in Figure

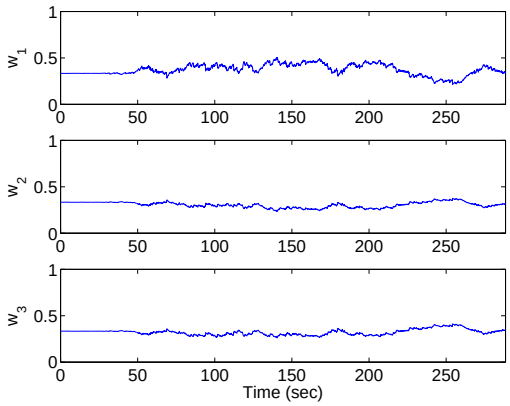

Figure 3. MMAE Filter Weights

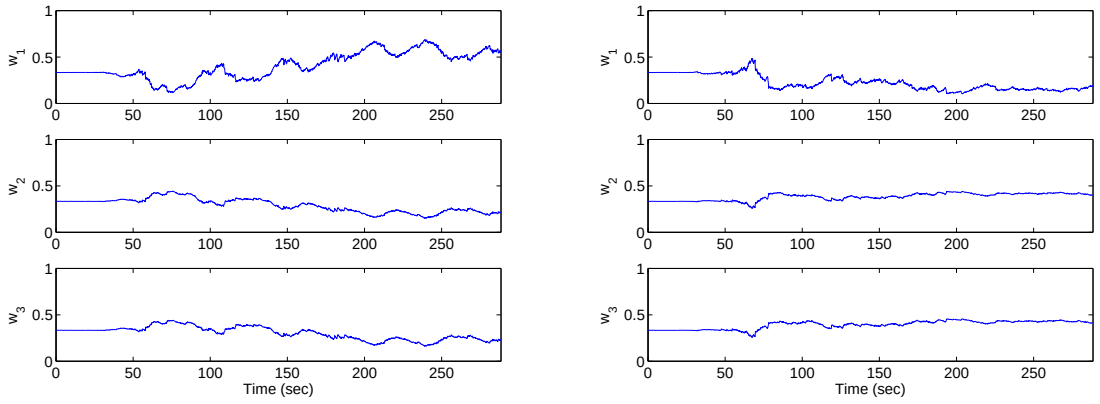

(a) +10 percent IC error

(b) -20 percent IC error

Figure 4. MMAE Weight Response Comparison

5(a). The attitude errors converge to small values since a significant amount of vehicle motion is present. These errors are within their respective 3σ bounds, which indicates that the MMAE is performing correctly. The position errors are shown in Figure 5(b), which are also within their respective 3σ bounds. Gyro and accelerometer bias errors are shown in Figures 5(c) and 5(d), respectively. Gyro and accelerometer scale factor errors are shown in Figures 5(e) and 5(f), respectively. The simulation shows that good performance characteristics can be obtained using an MMAE scheme for INS estimation, assuming that accurate initial attitude, position and velocity are known.

The key features of the proposed MMAE schemes, which make them attractive to future Mars or Moon landing missions, include, but are not limited, to the following:

1. It provides an autonomous and adaptive mixing capability that employs separate state estimate vectors produced by three filters to ensure that the navigation solution accuracy is bounded and stays within the pinpoint landing criterion (i.e., less than 1 kilometer).

2. The ability to adaptively compensate for operating condition uncertainties (as shown in Figure 4 versus the baseline condition shown in Figure 3) by knowing exactly how much information each filter should provide so that the overall MMAE scheme continuously keeps the navigation solution accuracy to stay within the pinpoint landing requirement. As shown in Figure 3 for the baseline operating condition defined earlier, the state estimate vectors of the three filters are almost equally weighted. On the other hand, for the two cases shown in Figure 4 corresponding to IC conditions uncertainties, due to entry navigation knowledge fluctuation, the MMAE weights' responses reflect a different weight value per filter. For example Figure 4(a) shows that filter 1's state vector has been weighted more than that of filters 2 and 3, which illustrates that the MMAE scheme knows exactly how to mix the state estimates among the three filters in order to maintain its acceptable navigation solution accuracy. This feature is definitely more attractive than a single EKF scheme, because during EDL the dynamics of the state vector itself is continuously and constantly changing (i.e., magnitudes of acceleration, rate, and velocity components) and there is no clear cut time instant at which a single filter can effectively handle the overlapping condition. Therefore, some state estimate information will be lost under the single EKF implementation (due to the "or" logic for a single EKF filter implementation, i.e. "if rate is high, use filter 3, else if rate is medium, use filter 2, else use filter 1"). It is challenging to determine where the right cut off should be for high, medium, or low conditions using a manual filter switch implementation logic. As a result, MMAE is a better choice for the navigation system design of future space missions because of its robust performance and autonomous adaptation.

3. The MMAE is also attractive for the situation where mixing of multiple external aiding sources is needed in order to continuously correct the IMU errors and to enhance the navigation solution accuracy. The multiple filter structure lends itself to a natural multiple aiding sensor fusion using the mixing scheme of the MMAE weights. As discussed in item 2, the MMAE weights are optimally and dynamically adjusted in realtime to maintain the overall fusion estimate optimal with respect to the Bayesian criterion (to account for disparate sensor sources and uncertainties).

IX. Conclusions

In this paper an MMAE filter formulation was derived for the purpose of INS applications during Mars entry. Simulation results indicated that the performance of the MMAE filter depends on the weighting of three extended Kalman filters (EKFs): a 9 state EKF, which includes attitude, position and velocity states, a 15 state EKF, which adds gyro and accelerometer biases to the EKF's state vector to account for "medium" magnitude range of operating conditions for the rate and velocity vectors, and a 21 state EKF, which adds gyro and accelerometer scale factors to the state vector to compensate for the high rate and acceleration operating conditions. The results reaffirm the notion of information dilution since each filter plays a part in the overall estimation process.

Acknowledgements

The authors would like to thank Dr. Michael E. Lisano from the Jet Propulsion Laboratory for many helpful suggestions and comments.

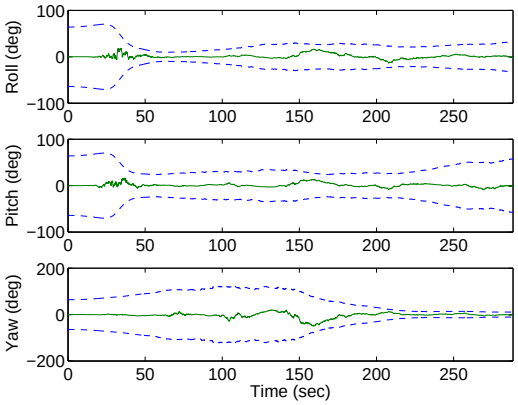

(a) Attitude Errors and 3σ Bounds

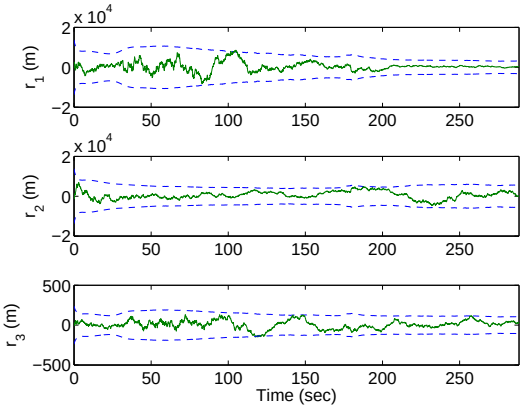

(b) Position Errors and 3σ Bounds

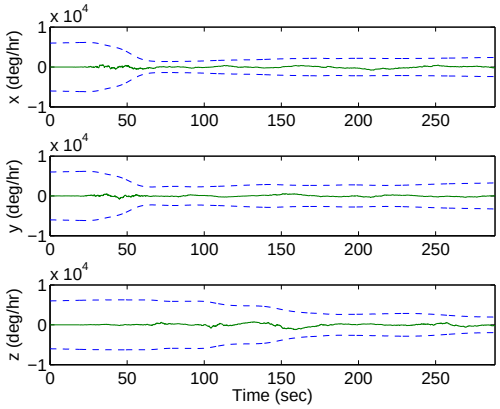

(c) Gyro-Bias Errors and 3σ Bounds

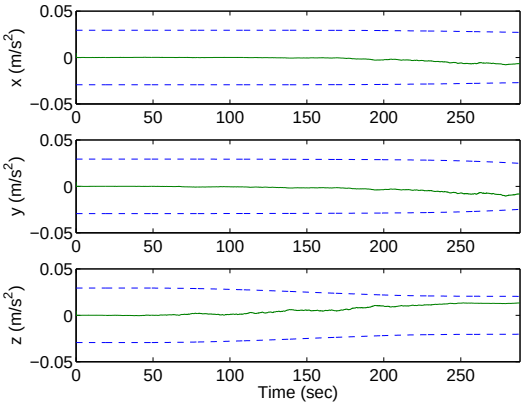

(d) Accelerometer-Bias Errors and 3σ Bounds

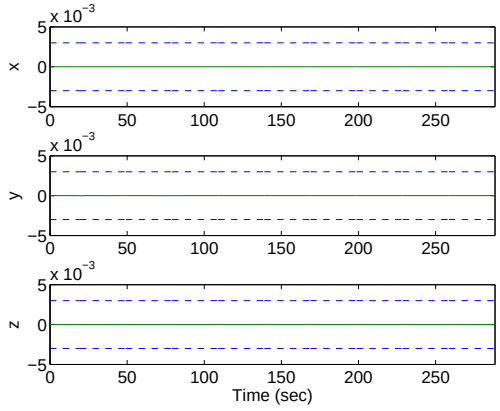

(e) Gyro-Scale Factor Errors and 3σ Bounds

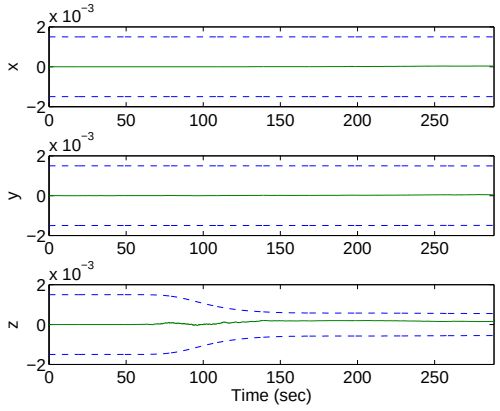

(f) Accelerometer-Scale Factor Errors and 3σ Bounds

Figure 5. MMAE Filter Results

References

[1]Lam, Q. and Crassidis, J. L., "Precision Attitude Determination Using a Multiple Model Adaptive Estimation Scheme," *IEEE/AIAA Aerospace Conference*, Big Sky, MT, March 2007, IEEEAC Paper #1439.

[2]Lam, Q. and Crassidis, J. L., "Evaluation of a Multiple Model Adaptive Estimation for Space Vehicle's Enhanced Navigation Solution," *AIAA Guidance, Navigation, and Control Conference*, Hitlon Head, SC, Aug. 2007, AIAA-02-6816.

[3]Zanetti, R. and Bishop, R. H., "Adaptive Entry Navigation Using Inertial Measurements," *AAS/AIAA Space Flight Mechanics Meeting*, Sedona, AZ, Jan.-Feb. 2007, AAS-07-129.

[4]Rapoport, I. and Bar-Itzhack, I. Y., "On The Information Dilution Theorem and Its Application to Attitude Determination," *Journal of the Astronautical Sciences*, Vol. 49, No. 3, July-Sept. 2001, pp. 489–508.

[5]Shuster, M. D., "A Survey of Attitude Representations," *Journal of the Astronautical Sciences*, Vol. 41, No. 4, Oct.-Dec. 1993, pp. 439–517.

[6]Hamilton, W. R., *Elements of Quaternions*, Longmans, Green and Co., London, England, 1866.

[7]Lefferts, E. J., Markley, F. L., and Shuster, M. D., "Kalman Filtering for Spacecraft Attitude Estimation," *Journal of Guidance, Control, and Dynamics*, Vol. 5, No. 5, Sept.-Oct. 1982, pp. 417–429.

[8]Shepperd, S. W., "Quaternion from Rotation Matrix," *Journal of Guidance and Control*, Vol. 1, No. 3, May-June 1978, pp. 223–224.

[9]Kuipers, J. B., *Quaternions and Rotation Sequences: A Primer with Applications to Orbits, Aerospace, and Virtual Reality*, Princeton University Press, Princeton, NJ, 1999.

[10]Crassidis, J. L., "Sigma-Point Kalman Filtering for Integrated GPS and Inertial Navigation," *AIAA Guidance, Navigation and Contol Conference*, San Francisco, CA, Aug. 2005, AIAA-2005-6052.

[11]Lightsey, E. G., Mogensen, A. E., Burkhart, P. D., Ely, T. A., , and Duncan, C., "Real-Time Navigation for Mars Missions Using the Mars Network," *Journal of Spacecraft and Rockets*, Vol. 45, No. 3, May-June 2008, pp. 519–533.

[12]van Loan, C. F., "Computing Integrals Involving the Matrix Exponential," *IEEE Transactions on Automatic Control*, Vol. AC-23, No. 3, June 1978, pp. 396–404.

[13]Brown, R. G. and Hwang, P. Y. C., *Introduction to Random Signals and Applied Kalman Filtering*, John Wiley & Sons, New York, NY, 3rd ed., 1997, pp. 353–361.

[14]Stengel, R. F., *Optimal Control and Estimation*, Dover Publications, New York, NY, 1994, pp. 402–407.

[15]Anderson, B. D. O. and Moore, J. B., *Optimal Filtering*, chap. 10.1, Dover Publications, Mineola, NY, 2005.

[16]Anderson, B. D. O., Moore, J. B., and Hawkes, R. M., "Model Approximations via Prediction Error Identification," *Automatica*, Vol. 14, No. 6, Nov. 1978, pp. 615–622.